ELSEVIER

International Journal of Heat and Fluid Flow 23 (2002) 639–646

International Journal of HEAT AND FLUID FLOW

www.elsevier.com/locate/ijhff

Interaction between particle clusters and particle-induced turbulence

Takeo Kajishima *, Saotshi Takiguchi [1]

Department of Mechanical Engineering, Osaka University, Yamadaoka, Suita, Osaka 565-0871, Japan

Abstract

To investigate the two-way interaction between particles and fluid turbulence, a homogeneous flow field including solid particles was numerically simulated. Spherical particles are falling by gravity with the Reynolds number ranging from 50 to 400, based on slip velocity. Particular attention was focused on the clustering of particles, which might enhance turbulence by energy supply through larger scales in comparison with dispersed particles. In the higher Reynolds number case, particle clusters are formed due to the wake, and vortex shedding enhances them. But clusters cause fluid turbulence resulting in their break-up. The Reynolds-number dependence, the dynamics and the time scale of particle clusters are discussed in this paper. © 2002 Elsevier Science Inc. All rights reserved.

Keywords: Multiphase flow; Turbulent flow; Particle-laden turbulence; Wake; Turbulence modulation; Direct numerical simulation

1. Introduction

Solid particles affect the turbulence transport of momentum, heat and mass in nature and industrial applications. Experimental and numerical investigations have therefore been conducted for a wide variety of flows. Some maps have been proposed to predict the turbulence modulation due to solid particles (Gore and Crowe, 1989; Elghobashi, 1994). Parameters used in them were not universal, however, probably, because the mechanism was not understood completely. We believe direct numerical simulation (DNS) is suitable to reveal vortex structures dominating the turbulence modulation.

The objective of our study is to improve turbulence models and particle-tracking methods for the unsteady simulation of particle-laden flows. Especially for industrial and geophysical interests, we intend to develop the applicability of numerical simulation to flows including many solid particles moving at relatively high Reynolds number of $\mathcal{O}[10^2]$, based on slip velocity and particle diameter.

Hereafter, we consider uni-scale spheres as solid particles. Even for the most fundamental case, in which a sphere is fixed in a uniform stream, the flow pattern changes drastically in the above-mentioned Reynolds number range as observed experimentally (Achenbach, 1974; Sakamoto and Haniu, 1990) as well as numerically (Shirayama, 1992; Johnson and Patel, 1999). Fig. 1 shows typical examples of unsteady vortex shedding obtained by our method (Takiguchi et al., 1999; Kajishima et al., 1999, 2001) developed prior to this study. The Reynolds-number dependence of flow patterns as well as the time-averaged drag is in good agreement with experimental data.

As shown in Fig. 1, unsteady vortex shedding takes place when the Reynolds number Re_{ps} exceeds approximately 300. The orientation of shed vortices alters slightly at $Re_{ps} = 400$. The period and shape of vortices are becoming more irregular for $Re_{ps} \geqslant 500$.

When vortex shedding from solid particles takes place, turbulence energy induced through the wake is not fully dissipated in the region near a particle. We estimated that approximately 20% of particle work becomes an additional source of turbulence energy through vortex shedding (Kajishima et al., 1999). However, uniformly distributed particles attenuate turbulence since wakes reduce the length-scale of background turbulence and modify it to a more dissipative structure. On the other hand, turbulence is augmented when non-uniformity of particle distribution increases because turbulence energy is supplied at larger scale.

* Corresponding author.

E-mail addresses: kajisima@mech.eng.osaka-u.ac.jp (T. Kajishima), takiguti@ws.trdc.mhi.co.jp (S. Takiguchi).

[1] Present address: Mitsubishi Heavy Industries, Ltd., Arai-cho, Takasago 676-8686, Japan.

0142-727X/02/$ - see front matter
PII: S0142-727X(02)00159-5

Nomenclature

C_D	drag coefficient
D_p	diameter of spherical particle
$\boldsymbol{f}_p$	momentum exchange in the interface cell
N_p	numbers of solid particles
N_x, N_y, N_z	numbers of grid points
p	pressure
Re_p	particle Reynolds number based on slip velocity and diameter
Re_{ps}	particle Reynolds number (setup)
t_p	particle response time (Stokes)
$\boldsymbol{u}_f$	velocity of fluid
$\boldsymbol{v}_p$	velocity of particle
u, v	velocity components in horizontal direction
w	velocity component in vertical direction
x, y	horizontal directions
z	vertical direction
α	volumetric fraction of solid in the interface cell
Δ	grid spacing
Δt	time increment
ε_p	volumetric fraction of particles
ϕ_p	mass loading ratio of particles
ρ	density
ν	kinematic viscosity
$\boldsymbol{\tau}$	fluid stress
$\boldsymbol{\omega}_p$	angular velocity of particle

Subscripts

f	fluid
p	solid particle

On the basis of above-mentioned observations, we considered the particle Reynolds number and the inter-particle distance as important factors of particle effects on turbulence (Kajishima et al., 1999). To parameterize them, we must clarify the dynamics of particle clusters and its interaction with fluid turbulence.

The region with high concentration of particle is sometimes referred to as the cluster. Note that particles in the cluster are not always in contact with one another. There have been some possible explanations for the mechanism of clustering—for example, preferential concentration of particles in particular portion of turbulence eddies (realized numerically by Eaton and Fessler, 1994, for example) and inelastic collision between particles (Goldhirsch and Zanetti, 1993, for example). The former is observed for small (low Stokes number) particles and the latter is an inter-particle effect. Thus, the interaction between solid particles and fluid turbulence is not so important in these cases. However, the two-way interaction is essential in the Reynolds number range of interest to us, $\mathcal{O}[10^2]$.

In this study, we investigate the dynamics of the wake-induced clusters of particles and the interaction between particles and fluid flow by means of DNS. In Section 2, the numerical scheme for two-way coupling and the computational setups are explained. In Section 3, the Reynolds-number dependence and life cycle of particle clusters are revealed on the basis of DNS. Finally in Section 4, concluding remarks will be given.

2. Computational method

To deal with $\mathcal{O}[10^2]$ range of particle Reynolds number, we developed an efficient two-way-coupling scheme based on the finite-difference method (Takiguchi et al., 1999; Kajishima et al., 1999, 2001). In our calculation, the flow around a number of moving particles is directly resolved, and the particle motion is described by the surface integral of fluid stress together with body force such as gravity. It is therefore a more complete DNS than previous methods using point-source models (Maxey and Riley, 1983; Elghobashi and Truesdell, 1992).

As the detail of numerical method has been given in an earlier paper (Kajishima et al., 2001), only an outline is given here. The computational mesh, cubic in this study, does not fit the surface of spherical particles. The volume fraction of the particle in the cell, including solid–fluid interface, is taken into account.

The volume-weighted average of velocity

$$\boldsymbol{u} = (1-\alpha)\boldsymbol{u}_f + \alpha\boldsymbol{u}_p, \tag{1}$$

is introduced for two-way coupling. In Eq. (1), α represents the volumetric fraction of the solid in the computational cell, $\boldsymbol{u}_f$ the fluid velocity, $\boldsymbol{u}_p(=\boldsymbol{v}_p+\boldsymbol{r}\times\boldsymbol{\omega}_p)$ the velocity inside the solid particle, $\boldsymbol{v}_p$ the particle velocity and $\boldsymbol{\omega}_p$ the angular velocity. Based on the Navier–Stokes equation for $\boldsymbol{u}_f$, a governing equation for $\boldsymbol{u}$ is given as

$$\frac{\partial \boldsymbol{u}}{\partial t} = -\nabla\frac{p}{\rho_f} - \boldsymbol{u}\cdot\nabla\boldsymbol{u} + \nu_f\nabla^2\boldsymbol{u} + \boldsymbol{f}_p. \tag{2}$$

The additional term,

$$\boldsymbol{f}_p = \alpha\left(\boldsymbol{u}_p - \widehat{\boldsymbol{u}}_f\right)/\Delta t, \tag{3}$$

is given at the cell, including the solid–fluid boundary. First, the unsteady equation for fluid flow

$$\frac{\partial \boldsymbol{u}_f}{\partial t} = -\nabla\frac{p}{\rho_f} - \boldsymbol{u}_f\cdot\nabla\boldsymbol{u}_f + \nu_f\nabla^2\boldsymbol{u}_f, \quad \nabla\cdot\boldsymbol{u}_f = 0 \tag{4}$$

is solved as if the field were occupied by fluid, and the result is denoted by $\widehat{\boldsymbol{u}}_f$. Next, $\boldsymbol{f}_p$ modifies $\widehat{\boldsymbol{u}}_f$ to $\boldsymbol{u}$ using a discretized form of Eq. (2), $\boldsymbol{u} = \widehat{\boldsymbol{u}}_f + \Delta t\boldsymbol{f}_p$. Thus, $\boldsymbol{f}_p$ is

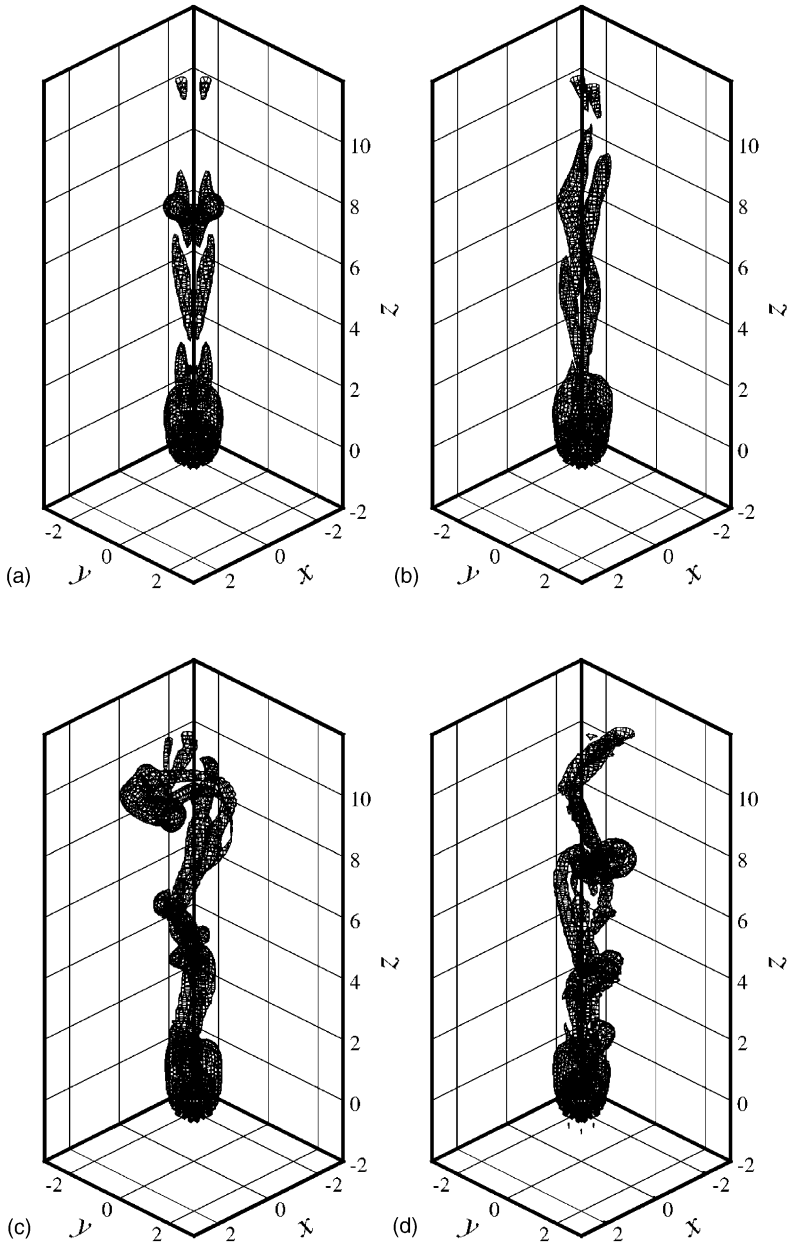

Fig. 1. Unsteady vortex shedding from a spherical particle fixed in a uniform stream: instantaneous vortex structures visualized by $\nabla^2 p$ iso-surfaces. $Re_{ps} = 300$ (a), 400 (b), 500 (c), 600 (d).

interpreted as the momentum exchange between the phases.

The surface integral of the fluid stress $\boldsymbol{\tau}$ in the equations for the particle can therefore be replaced by the volumetric integral of $\boldsymbol{f}_p$ as

$$\left.\begin{aligned} &\frac{d(m_p \boldsymbol{v}_p)}{dt}\left[= \int_{S_p} \boldsymbol{\tau}\cdot\boldsymbol{n}\, dS + \boldsymbol{G}_p \right] \\ &\quad = -\int_{V_p} \boldsymbol{f}_p\, dV + \boldsymbol{G}_p, \\ &\frac{d(\boldsymbol{I}_p\cdot\boldsymbol{\omega}_p)}{dt}\left[= \int_{S_p} \boldsymbol{r}\times(\boldsymbol{\tau}\cdot\boldsymbol{n})\, dS + \boldsymbol{N}_p \right] \\ &\quad = -\int_{V_p} \boldsymbol{r}\times\boldsymbol{f}_p\, dV + \boldsymbol{N}_p \end{aligned}\right\}, \tag{5}$$

where m_p denotes the mass of the particle, $\boldsymbol{I}_p$ the inertia tensor of the particle, S_p the particle surface, $\boldsymbol{n}$ the unit vector in the normal outward direction at the surface, and $\boldsymbol{r}$ the relative position from the center of rotation. The last two terms, $\boldsymbol{G}_p$ and $\boldsymbol{N}_p$, are external force and moment, respectively. The domain V_p is slightly larger than the particle, including all its interfacial cells. Since the grid for the fluid-flow simulation is used for the volumetric integral in Eq. (5), there is no residual in the momentum exchange between the two phases.

Hereafter in this study, we ignore the rotation of particles to reduce the computational complexity and cost.

Table 1
Numerical setup for DNS of homogeneous flow including falling particles.

		Case 1	Case 2
Number of grid points			
Horizontal	$N_x \times N_y$	256×256	512×512
Vertical	N_z	512	1024
Grid resolution for particle diameter			
	D_p/Δ	10	10
Properties of solid particles			
Number of solid particles	N_p	128	1024
Density ratio	ρ_p/ρ_f	10	8.8
Reynolds number	Re_{ps}	50–400	350
Stokes number	St_p	27.8–222	171
Volmetric fraction	ε_p	0.20%	0.20%
Mass loading ratio	ϕ_p	1.96%	1.73%

We apply our DNS method to homogeneous turbulence including spherical particles. The computational setup is summarized in Table 1. Grid points for the fluid turbulence simulation are distributed uniformly in a periodic computational domain. The spatial derivative is approximated by a fourth-order accurate central finite-difference method. Second-order schemes are applied for time marching, namely the Adams–Bashforth method for the equations of motion for fluid and solid particle and the Crank–Nicholson method for the particle movement. The SMAC method is used for velocity–pressure coupling in Eq. (4).

The ratio of particle diameter to grid spacing is 10, which allowed sufficient accuracy for vortex shedding at the particle Reynolds number range of interest (Kajishima et al., 2001). The number of particles is limited so that the volumetric fraction is 0.2%. In such a dilute mixture, inter-particle collisions could occur, but are unlikely to dominate the particle distribution and the flow field. Thus, we assume elastic collisions for simplicity in this study. The density of particles is assumed to be about 10 times larger than that of fluid. Hence, particles fall down by gravity. To keep the mass flow rate of the mixture to zero, we adjusted the vertical gradient of pressure in the equation of fluid motion.

The Reynolds number Re_{ps} in Table 1 is adjusted by changing the fluid viscosity so that the gravity and drag are in balance. This is based on the particle diameter and the terminal velocity when a particle falls in a stationary and infinite domain. The drag is estimated by the standard Re_{ps}–C_D curve for a fixed sphere in a uniform flow (Clift et al., 1978). On the other hand, Re_p shown later is

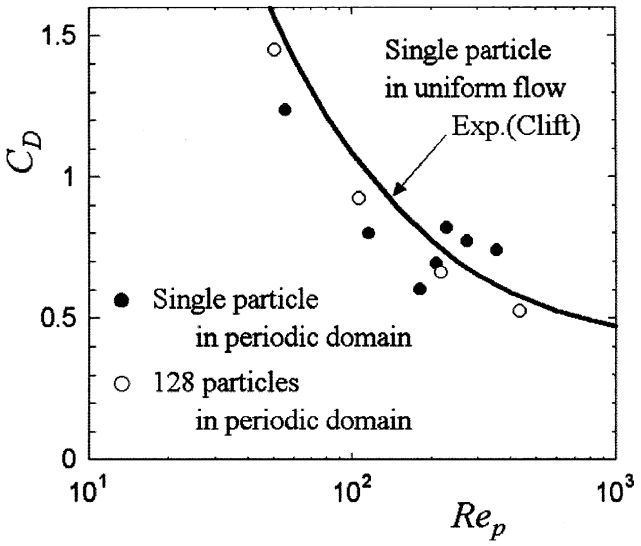

Fig. 3. Drag coefficient on a sphere: comparison among results for a single sphere fixed in a uniform stream, a single sphere in a periodic box, and falling spheres in a periodic box.

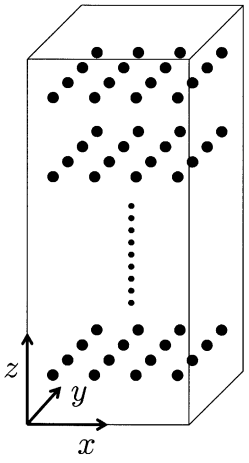

Fig. 2. Coordinates and initial conditions: fluid and particles are at rest.

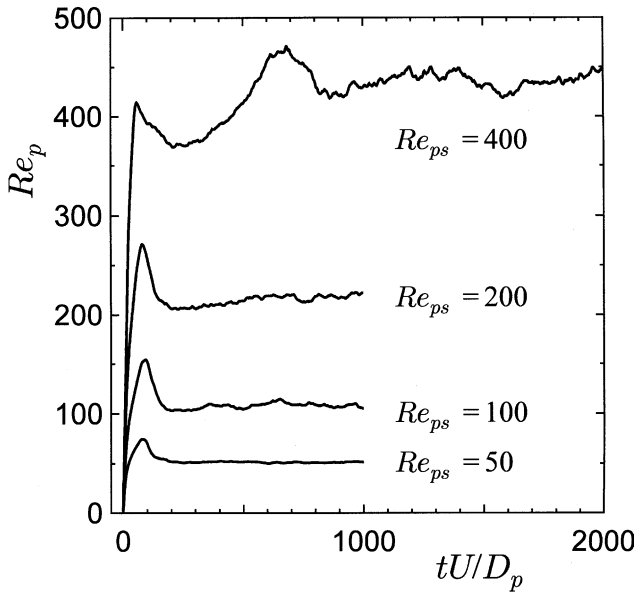

Fig. 4. Time evolution of averaged Reynolds number of falling particles.

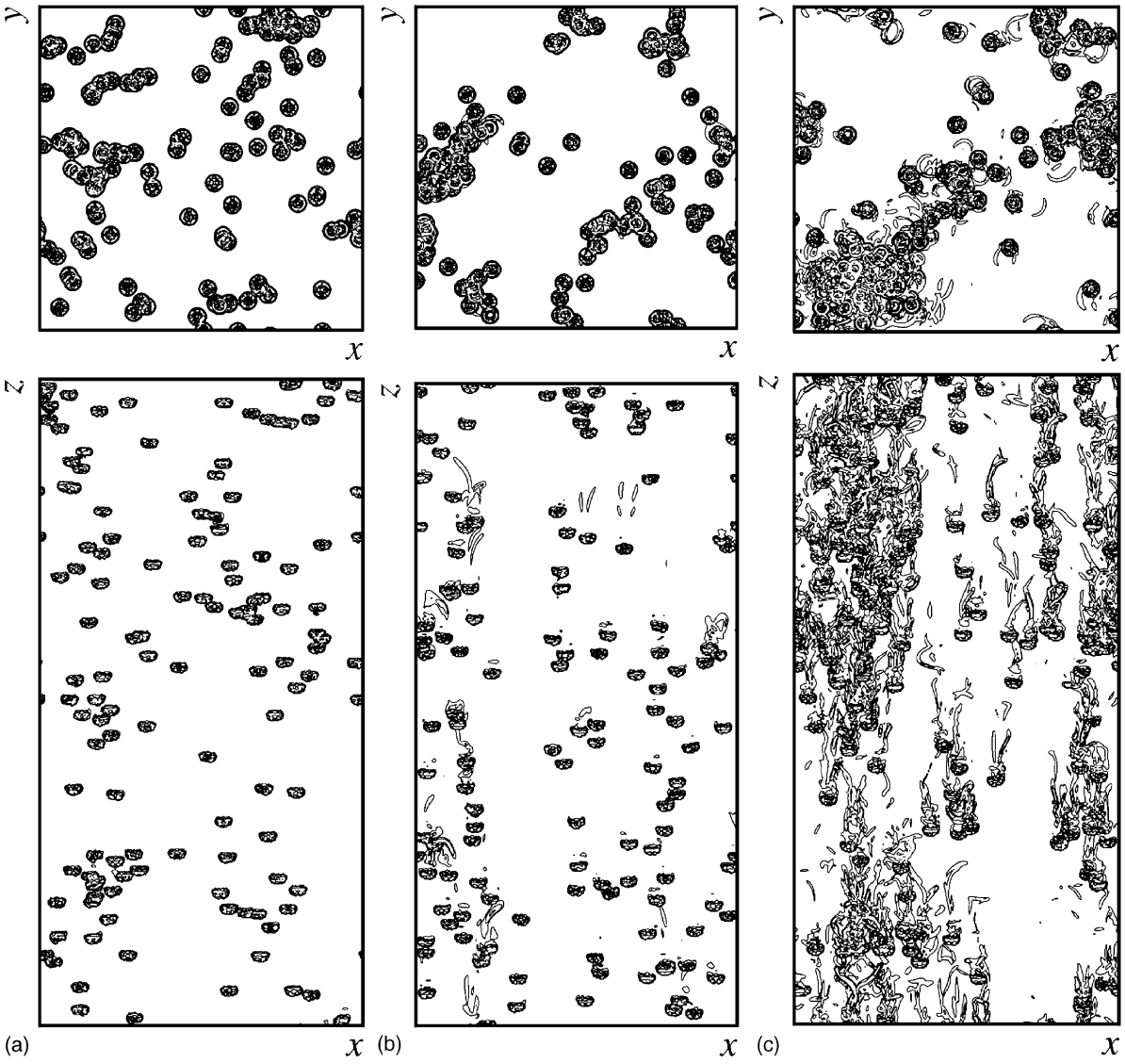

Fig. 5. Instantaneous flow field, including 128 falling particles, visualized by $\nabla^2 p$ projected in the horizontal (top row) and vertical (bottom row) planes. (a) $Re_{ps} = 100$, (b) $Re_{ps} = 200$ and (c) $Re_{ps} = 400$.

based on the average slip velocity between falling particles and fluid in a periodic domain. This is different from Re_{ps}.

To identify the influence of Reynolds number, we simulated four cases, $Re_{ps} = 50$, 100, 200 and 400 by Case 1. Initially, particles were arrenged in the manner shown in Fig. 2, and particles and fluid were at rest. Then the flow field was advanced in time to the fully developed state.

3. Results and discussion

Fig. 3 shows the relationships between drag coefficient C_D and particle Reynolds number Re_p. The drag on particles should be compared with that on a single particle subject to the same boundary condition, namely the periodicity assumption in all directions. The drag on a particle in a periodic box, which is identical to one of particles in the array, differs from that on a particle in a uniform stream, because of the influence of wakes of upstream particle. The result for a single particle, shown in Fig. 3, was obtained in the domain covered by $128 \times 128 \times 512$ grid points. At low Reynolds numbers, the drag is reduced due to lower velocity in the wake. At high Reynolds numbers, on the other hand, the drag is increased due to the fluctuation of the wake. As a consequence, the drag coefficient profile for a spherical particle in a periodic domain changes suddenly at around $Re_p = 200$–300.

The drag on particles trapped in the wake of upstream ones is likely to be smaller than those falling

individually. Thus, they approach ones present in lower position. This is the mechanism of clustering due to the wake. Since particles tend to form clusters at higher Reynolds numbers, C_D decreases in comparison with that for a single particle, as shown in Fig. 3.

Fig. 4 shows the Reynolds-number dependence on the time evolution of falling velocity. The decrease of C_D results in the increase in average Re_p. For higher Reynolds numbers, Re_p of falling particles increases beyond Re_{ps} and fluctuates with time. Particles at lower Reynolds numbers, $Re_{ps} = 50$ and 100, on the other hand, fall with almost constant velocity.

Fig. 5 compares instantaneous flow fields including particles. Particles at $Re_{ps} = 100$ are dispersed. Thus, only vortex rings attached to particles are visualized in Fig. 5(a). In contrast, particles at $Re_{ps} = 400$ form clusters as illustrated in Fig. 5(c). For $Re_{ps} > 300$, the C_D value for single particles increases, as shown in Fig. 3, but the wake including vortex shedding attracts other particles far downstream. For lower Re_{ps}, on the other hand, inter-particle interaction through wakes is not so evident in such a dilute case. As for intermediate Reynolds numbers, single particles at $Re_{ps} = 200$ do not shed vortices. But the particles form small clusters, as shown in Fig. 5(b), and some of them shed vortices similarly to a particle with a higher Reynolds number. We believe the monotonous decrease in C_D shown in Fig. 3 is the consequence of a continuous increase in size and/or number of clusters with Re_{ps}, as shown in Fig. 5.

Fig. 6 shows the three-dimensional spectrum of horizontal velocity fluctuation u'_f (and v'_f). With increasing Re_{ps}, the energy increases at first in the low wave number range and then in the higher wave-number range. The former is due to the increase in non-uniformity of particle distribution, while the latter is due to the vortex shedding. In addition, for $Re_{ps} = 400$, the energy at the smallest wave-number end in our computational domain still grows due to the growing cluster.

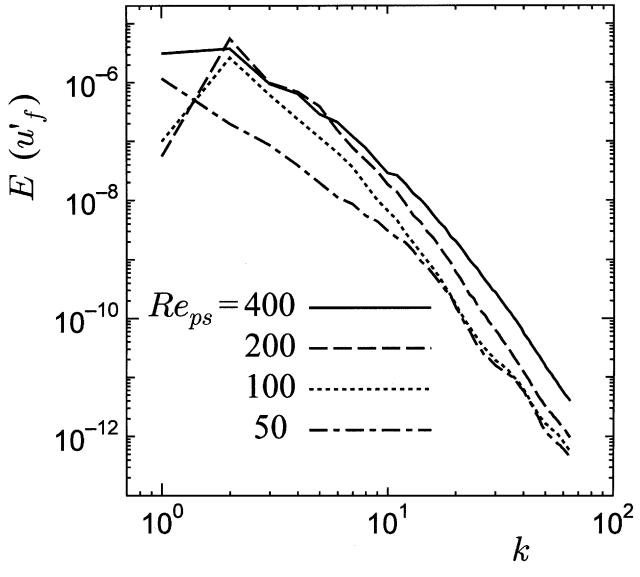

Fig. 6. Three-dimensional spectrum of horizontal velocity fluctuations.

Fig. 7 shows a top view of the time evolution of the particle distribution for the interval of particle response time t_p in the case of $Re_{ps} = 400$. Clusters grow in size, move and break up. Our computational domain is sufficient for the observation of particle clusters, but seems somewhat small for analyzing cluster–cluster or cluster–turbulence interactions.

To consider the life cycle of particle clusters, the relationship between particle motion and intensity of fluid turbulence are shown in Fig. 8. Due to lower drag on particles in the cluster, they fall faster than the terminal velocity of single particles. So we can detect the cluster by the particle Reynolds number Re_p. At $t = 3t_p$, the maximum of Re_p shown in Fig. 8 is due to four small clusters observed in Fig. 7. Then they are re-arranged to form larger ones. A cluster causes a downward current of fluid moving with it. As shown in Fig. 8, the vertical fluctuation of fluid velocity w'_f synchronizes with Re_p and the horizontal component u'_f also does so with a slight delay through the redistribution among components of velocity fluctuation. The turbulent shear stress around clusters is consequently intensified and resists the cluster motion, resulting in a break-up of the cluster. This is a life cycle of a particle cluster in the homogeneous flow.

Spatial and temporal scales of clusters may depend on the particle response time t_p, the particle loading ratio ε_p and the background turbulence. In our particular case, without extra source of turbulence other than the existence of particles, the period from clustering to break-up is supposed to be several times larger than t_p, as shown in Fig. 8. Of course, a series of computation is required to parameterize the cluster dynamics for a wider range of conditions.

Finally, a typical example obtained by a larger scale computation is shown in Fig. 9. In Case 2, the domain was enlarged to be twice that of Case 1 in each direction. Thus, the number of grid points is $512^2 \times 1024$, and the number of particles is $N_p = 1024$ for the same volumetric fraction. The memory requirement for Case 2 was 32.2 GB. The particle properties, $Re_{ps} = 350$ and $\rho_p/\rho_f = 8.8$, are slightly different from those in abovementioned case, but the result is qualitatively close to that for $Re_{ps} = 400$. A comparison of Figs. 7 and 9(a) shows that the horizontal scale is not seriously affected by the domain size even in the smaller computation. We therefore believe the discussions on the Reynolds-number dependence of the particle distribution and the life cycle of particle clusters in this paper are reliable.

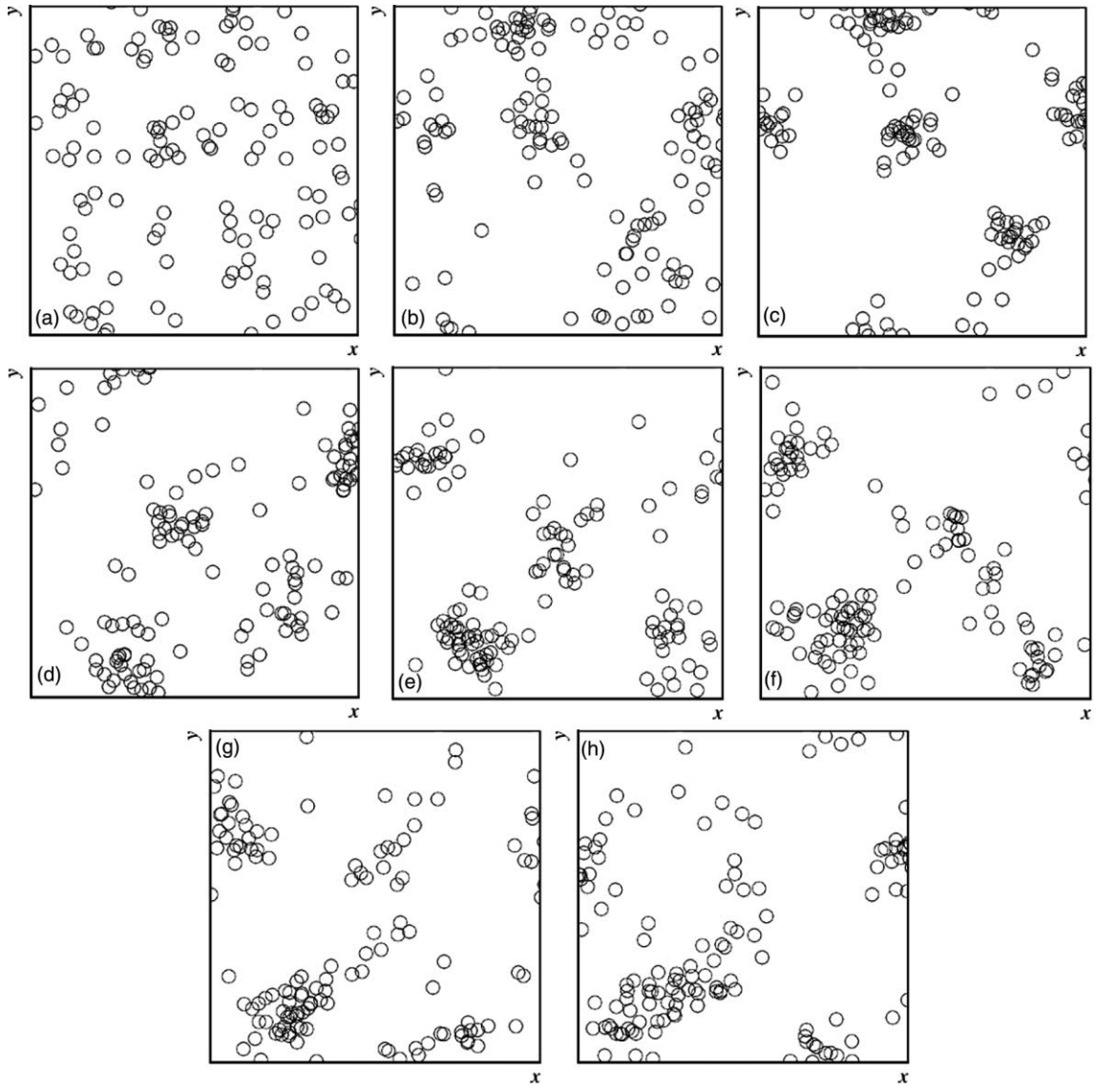

Fig. 7. Time evolution of particle distribution (top view, $Re_{ps} = 400$). $t = t_p$ (a), $2t_p$ (b), $3t_p$ (c), $4t_p$ (d), $5t_p$ (e), $6t_p$ (f), $7t_p$ (g), $8t_p$ (h).

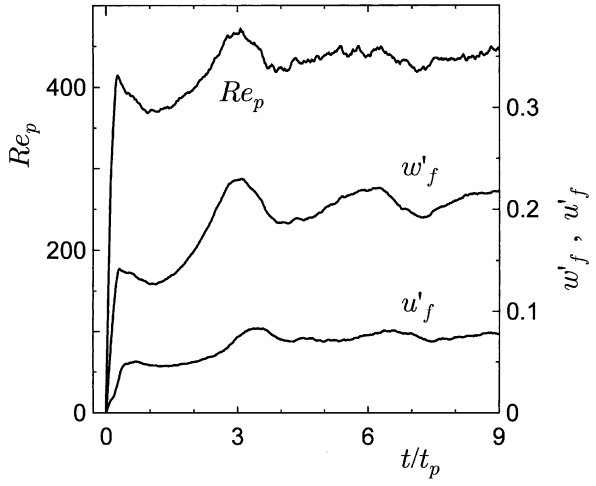

Fig. 8. Time evolutions of mean particle Reynolds number and turbulence intensities in vertical and horizontal directions ($Re_{ps} = 400$).

4. Conclusions

DNS was used to reproduce particle clustering, in particular the formation of high-concentration regions of solid particles in homogeneous flow field. Since clusters were caused by wakes from particles in our case, a scheme to resolve the flow around all particles was essential. Clusters grew with particle Reynolds number, especially in the values exceeding 300. Particle clusters induced large-scale eddies into the fluid flow and finally broke up due to the turbulence stress generated around them. The period from growing to break-up seemed to be a function of particle response time for the case without background turbulence.

Our result suggests that the turbulence energy induced through particle wakes, the scale of particles clusters and the Reynolds-number dependence of them

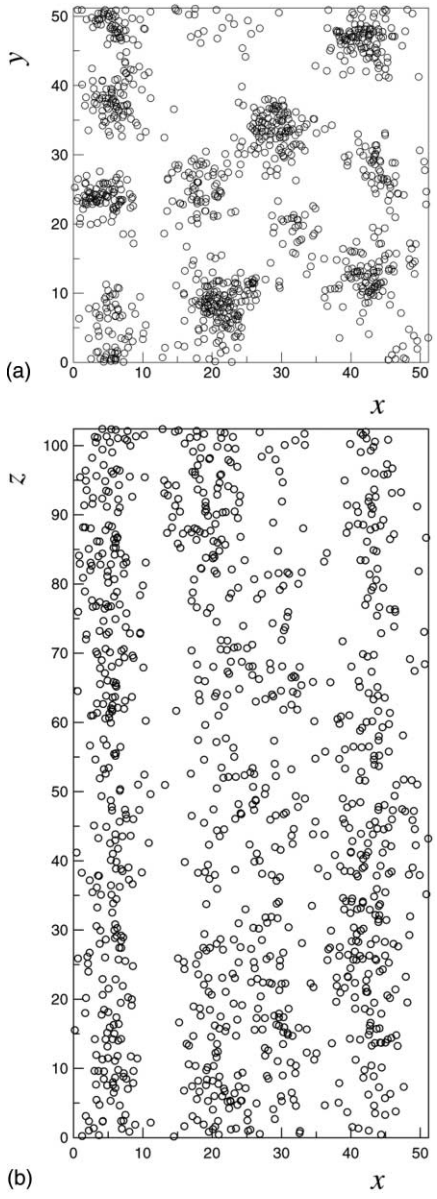

Fig. 9. Instantaneous distribution of 1024 particles ($Re_{ps} = 350$, $\rho_p/\rho_f = 8.8$). The number of grid points in each direction is $N_x = N_y = 512$ and $N_z = 1024$. (a) Top view, (b) side view.

are important factors in improving turbulence models for particle-laden fluid flow.

We finally displayed a scale-up simulation in Fig. 9. It proves that the size and behavior of particle cluster discussed in this paper are not strongly affected by the size of computational domain. In addition, cluster–cluster interaction phenomena are coming into view by the larger computation. Hence, we intend to increase the scale range of DNS to observe the interaction between solid particles and fluid turbulence for a better understanding of the turbulence–modulation mechanism.

Acknowledgements

This work has been partially supported by a Grant-in-Aid for Science Research on Priority Areas (B), no.12125202, from the Ministry of Education, Culture, Sports, Science and Technology of Japan.

References

Achenbach, E., 1974. Vortex shedding from spheres. J. Fluid Eng. 62 (2), 209–221.

Clift, R., Grace, J.R., Weber, M.E., 1978. Bubbles, Drops, and Particles. Academic Press, New York.

Eaton, J.K., Fessler, J.R., 1994. Preferential concentration of particles by turbulence. Int. J. Multiphase Flow 20 (Suppl), 169–209.

Elghobashi, S., Truesdell, G.C., 1992. Direct simulation of particle dispersion in a decaying isotropic turbulence. J. Fluid Mech. 242, 655–700.

Elghobashi, S., 1994. On predicting particle-laden turbulent flows. Appl. Sci. Res. 52, 309–329.

Goldhirsch, I., Zanetti, A., 1993. Clustering instability in dissipative gases. Phys. Rev. Lett. 70 (11), 1619–1622.

Gore, R.A., Crowe, C.T., 1989. Effect of particle size on modulating turbulence intensity. Int. J. Multiphase Flow 15 (2), 279–285.

Johnson, T.A., Patel, V.C., 1999. Flow past a sphere up to Reynolds number 300. J. Fluid Mech. 378, 19–70.

Kajishima, T., Takiguchi, S., Miyake, Y., 1999. Modulation and subgrid scale modeling of gas-particle turbulent flow. In: Knight, D., Sakell, L. (Eds.), Recent Advances in DNS and LES. Kluwer Academic Publishers, Dordrecht, pp. 235–244.

Kajishima, T., Takiguchi, S., Hamasaki, H., Miyake, Y., 2001. Turbulence structure of particle-laden flow in a vertical plane channel due to vortex shedding. JSME Int. J. Ser. B 44 (4), 526–535.

Maxey, M.R., Riley, J.J., 1983. Equation of motion for a small rigid sphere in a nonuniform flow. Phys. Fluids 26 (4), 883–889.

Sakamoto, H., Haniu, H., 1990. A study on vortex shedding from spheres in a uniform flow. Trans. ASME, J. Fluids Eng. 112, 386–392.

Shirayama, S., 1992. Flow past a sphere: topological transitions of the vorticity field. AIAA J. 30 (2), 349–358.

Takiguchi, S., Kajishima, T., Miyake, Y., 1999. Numerical scheme to resolve the interaction between solid-particles and fluid-turbulence. JSME Int. J. Ser. B 42 (3), 411–418.